RSC Advances

COMMUNICATION

Controlled growth of hexagonal Zn_2GeO_4 nanorods on carbon fibers for photocatalytic oxidation of *p*-toluidine†

Cite this: *RSC Adv.*, 2015, **5**, 25801

Received 1st February 2015
Accepted 6th March 2015

DOI: 10.1039/c5ra01972a

www.rsc.org/advances

Guohua Jiang,*[abc] Bolin Tang,[ab] Hua Chen,[ab] Yongkun Liu,[ab] Lei Li,[ab] Qin Huang[ab] and Wenxing Chen[abc]

In this paper, hexagonal Zn_2GeO_4 nanorods grown on the surface of carbon fibers (CFs) that were pre-activated by sodium hypochlorite were prepared by a facile solvothermal method. The possible growth mechanism has been investigated by theoretical calculations and a simulation experiment by growth of Zn_2GeO_4 on a 2D flat surface of graphene. The (113) crystal facet of Zn_2GeO_4 nanorods attached to the CFs surface was the most stable structure. Due to the synergistic effect between the photocatalytic activity of Zn_2GeO_4 and excellent adsorption capacity of CFs, the resultant Zn_2GeO_4/CFs composites exhibited excellent photocatalytic activity for oxidation of *p*-toluidine.

In the past decades, semiconductor photocatalysis has attracted considerable attention owing to its application in environmental purification,[1] water splitting,[2] and conversion of solar energy into electrical energy,[3] *etc.* It is well known that when the surface of a semiconductor absorbs photons and its energy is equal to or higher than that of the band gap. The low-energy electrons of the valence band will be excited to the conduction band, and electron–hole pairs will be produced on the surface of the semiconductor. A photo-excited electron has a higher reducing power, and a photo-excited hole has a higher oxidizing power. If these photo-excited electron–hole pairs do not recombine, they would conduct reduction and oxidation reactions, respectively.[4]

The development of highly selective and environmentally benign chemical conversion processes to synthesize chemical specialties is an important subject in green chemistry. Unfortunately, the required selectivity often comes at the expense of specially designed metal catalysts or reagents which have adverse environmental effects.[5] One encouraging approach is to use nontoxic catalysts such as semiconductor photocatalysts in the presence of sunlight, which is a safe and sustainable energy source, as a driving force for the reaction.[6] For example, aromatic nitro-compounds can be reduced in the presence of sacrificial electron donors.[7] The selective photocatalytic oxidation of amines to imines using molecular oxygen as oxidant was reported over an amine-functionalized metal–organic-framework photocatalyst.[8] Recently, the selective oxidation of alcohols was achieved under visible-light irradiation in a system containing dye-sensitized TiO_2 and nitroxyl radicals (such as 2,2,6,6-tetramethylpiperidinyloxyl, TEMPO).[9] *p*-Nitrotoluene belongs to the group of aromatic nitro compounds which have widely used in the dye pharmaceuticals pesticides and other organicsynthesis.[10] The photoinduced synthesis of *p*-nitrotoluene should attract considerable interest in view of pursuing environmentally 'benign' or 'green' synthesis, since it consumes low-energy photons and occurs under atmospheric pressure and at room temperature.

Zn_2GeO_4, as an important wide-band-gap semiconductor photocatalyst, has shown good activities for photocatalytic synthesis due to its optical and electrochemical properties.[11] Compared with the traditional photocatalysts, such as TiO_2 or CdS, Zn_2GeO_4 has a low toxicity, low cost, high photocatalytic activity and photostability.[12] Despite these advantages, the practical applications of semiconductor photocatalysts need to deal with their aggregation and separation.[13] To solve these problems, an ideal way is to grow or immobilize these photocatalytic nanoparticles on certain substrates. Carbon fibers (CFs) were a new class of flexible materials with high mechanical strength, superior electroconductibility and excellent corrosion resistance. Meanwhile, they could supply a large surface area, which is critical for nanostructure-based

[a]*Department of Materials Engineering, Zhejiang Sci-Tech University, Hangzhou 310018, P. R. China. E-mail: ghjiang_cn@zstu.edu.cn; Tel: +86 571 86843527*

[b]*National Engineering Laboratory for Textile Fiber Materials and Processing Technology (Zhejiang), Hangzhou 310018, P. R. China*

[c]*Key Laboratory of Advanced Textile Materials and Manufacturing Technology (ATMT), Ministry of Education, Hangzhou 310018, P. R. China*

† Electronic supplementary information (ESI) available: Details of materials, activation of carbon fibers (CFs), preparation of Zn_2GeO_4/CFs composites, characterization, computational methods (Fig. S1), photocatalytic oxidation of *p*-toluidine, the surface energy of various facets of rhombohedral phase Zn_2GeO_4 (Fig. S2), the absolute value of interaction energy for graphite surface and various facets of rhombohedral phase Zn_2GeO_4 (Fig. S3), the surface energies of various crystal faces of Zn_2GeO_4 and graphene (Table S1) and the photocurrent transient response plots and electrochemical impedance spectra (EIS) of as-prepared samples (Fig. S4). See DOI: 10.1039/c5ra01972a

photovoltaic technology.[14] Therefore, CFs have been widely investigated as substrates in field of nanometer materials. Herein, hexagonal Zn_2GeO_4 nanorods grown on the surface of activated CFs were prepared by a facile solvothermal method (see detail preparation section in ESI†). The possible growth mechanism had been investigated by theoretical calculation and simulation experiment. The resultant Zn_2GeO_4/CFs composites exhibited excellent photocatalytic activity for oxidation of *p*-toluidine.

Firstly, the morphologies of products were characterized by SEM analysis. The CFs substrates are uniformly and compactly covered by a large number of nanoparticles to form a rough surface, as shown in Fig. 1A, compared with the relatively smooth surface of pure CFs (Fig. 1B). From the SEM image of products (Fig. 1C), the rod-like nanoparticles grown radially on the surface of CFs is packed closely. Further magnification the SEM image of nanorods, the regular hexagonal prism geometric shape at the terminal of them can be observed (Fig. 1D). The side length of hexagonal is around 30–50 nm. For further analysis the nanorods structure, they can be broken away from CFs through ultrasonic treatment. The TEM image of nanorods is shown in Fig 1E. The length and diameter of nanorods are around 120 and 40 nm, respectively. The nanorods grow in the direction along the *c*-axis of the rhombohedral phenacite-type structure.[15] The selected area electron diffraction (SAED) image of nanorods shown in Fig 1F reveals the single-crystalline nature of hexagonal nanorods. It is interesting to note that the resultant composites based on nanorods self-assembled on the CFs substrate is flexible and soft, which would favor the separation, recovery and reuse of the catalysts.

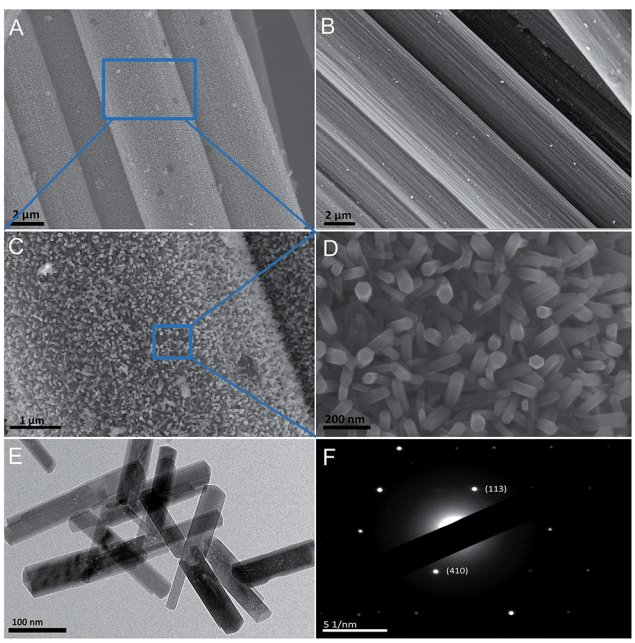

Fig. 1 SEM images of as-prepared Zn_2GeO_4/CFs with different magnification (A, C and D) and pristine CFs (B), TEM image of Zn_2GeO_4 nanorods that break away from CFs through ultrasonic treatment (E) and SAED image of Zn_2GeO_4 nanorods (F).

The crystalline phase of as-synthesized products was further identified by X-ray diffraction (XRD) measurement. As shown in Fig. 2A, it can be found that the pristine CFs exhibit a broad peak located between 20° and 30° assigned as the d_{002} layers, representing the presence of integral graphite crystal structure.[14] The as-synthesized products exhibit the typical diffraction peaks of rhombohedral Zn_2GeO_4, whose lattice parameters are $a = b = 14.231$, $c = 9.53$ Å (JCPDS 11-0687) except for the broad diffraction peak of pristine CFs. There is no trace of impurity phase under the instrument's resolution. The EDS of the products further confirms the existence of C, Zn, Ge and O elements (Fig. 2B).

As known to all, the formation of composites was considerably related to surface properties of basic materials.[16] For verification of the possible growth mechanism, the potential surface energy of contact surface of Zn_2GeO_4 and CFs were calculated by first-principles calculations by the generalized gradient approximation (GGA) (see Fig. S1 in ESI†). It can be found that the (410), (300) and (113) have the higher surface energies compared with other crystal facets (see Fig. S2 and Table S1 in ESI†). For further confirmation the preferential contact surface mentioned above, the interaction energies of CFs surface and Zn_2GeO_4 facets are estimated by constructed 3D periodic surface model of Zn_2GeO_4 and CFs. Generally, the interaction energy is estimated from the difference between the potential energy of the composites system, the potential energies for the crystal surfaces of Zn_2GeO_4 crystals and the corresponding graphene model.[17] The interactions of graphene and (113) facet of Zn_2GeO_4 is the strongest with an average interaction energy at -26.92 kcal mol^{-1} (see Fig. S3 and Table S1 in ESI†). It indicates that the contact between Zn_2GeO_4 (113) facet and CFs surface is the most stable. The crystal surface with high surface free energy act as nucleation sites to induce selective growth along a preferential growth direction.[18] Therefore, we believe that it is the high surface energy at Zn_2GeO_4 nanorods centers, along with the high mobility of deposited Zn_2GeO_4 species, that was responsible for the formation and growth of the rod-like structures onto surface of CFs reported in this work. To verify this hypothesis, the Zn_2GeO_4 nanorods grown on flat surfaces of 2D graphene were prepared under the same conditions to simulate preparation of Zn_2GeO_4/CFs. As shown in Fig. 3A, the large amount of Zn_2GeO_4 nanorods dispersed on the graphene can be observed. The heterojunction structure between Zn_2GeO_4 and graphene is shown in the HR-TEM image (Fig. 3B). The well-defined lattice fringes with the lattice spacing of 0.301 nm indexed to (113) plane of rhombohedral Zn_2GeO_4

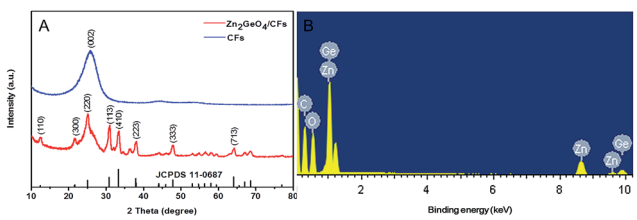

Fig. 2 XRD patterns of CFs and Zn_2GeO_4/CFs (A) and EDS spectrum of the as-prepared Zn_2GeO_4/CFs (B).

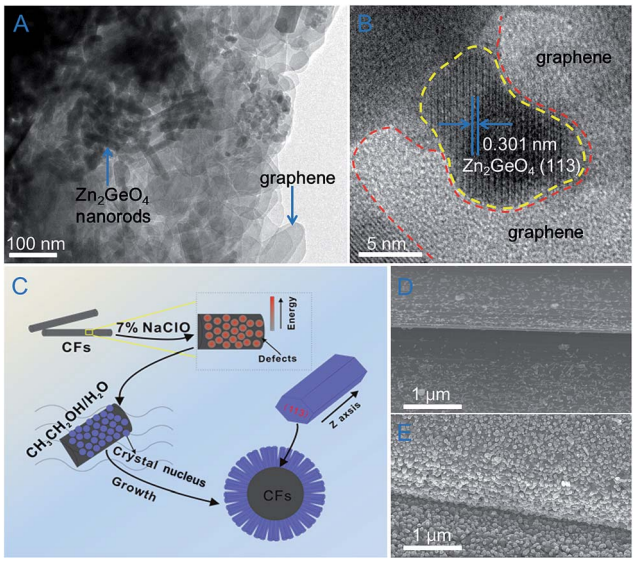

Fig. 3 TEM image of Zn_2GeO_4 nanorods dispersed on the graphene (A) and the *d*-spacing of (113) planes for Zn_2GeO_4 that attached onto the surface of 2D flat of graphene (B), the schematic representation for growth of Zn_2GeO_4 nanorods onto surfaces of CFs (C) and the SEM images of Zn_2GeO_4/CFs composites from pretreatment CFs by 30% H_2O_2 (D) or 5 M HNO_3 (E).

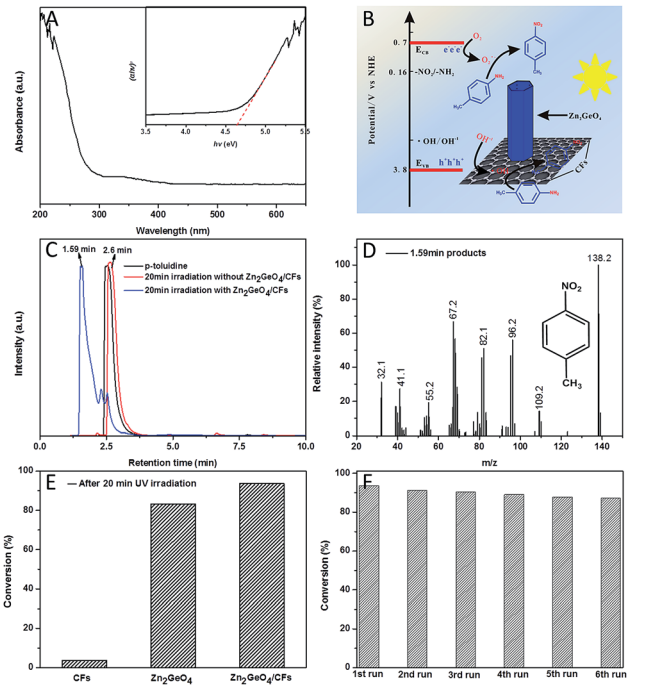

Fig. 4 UV-vis diffusion reflectance spectrum of Zn_2GeO_4/CFs (the inset shows the relationship between $(ah\nu)^2$ and photon energy) (A), schematic illustration of photocatalytic oxidation mechanism of the *p*-toluidine over Zn_2GeO_4/CFs composites under UV-light irradiation (B), HPLC of *p*-toluidine solutions after UV irradiation over Zn_2GeO_4/CFs composites (C), the mass spectrum of product with RRT at 1.59 min (D), the percent conversions (PC) for oxidation of *p*-toluidine over CFs, pure Zn_2GeO_4 and Zn_2GeO_4/CFs tested under the same conditions (E) and reusability of Zn_2GeO_4/CFs for oxidation of *p*-toluidine (F).

can be founded at the interface of graphene and edge of Zn_2GeO_4. It suggests (113) crystal faces of Zn_2GeO_4 nanorods is referential contact surfaces for the deposition and growth.

On the basis of above results and analysis, a reasonable mechanism for describing formation of Zn_2GeO_4/CFs composites is proposed, as shown in Fig. 3C. After the oxidation treatment using sodium hypochlorite with medium oxidation ability, the surface of CFs will obtain many defects. As is well known, surface defects with high surface free energy act as nucleation sites to induce selective growth along a preferential growth direction.[18] Zn_2GeO_4 crystals will grow preferentially from these high-energy sites. To minimize their surface energy, the high-energy (113) facets of Zn_2GeO_4 crystal will attach selectively to high-energy sites of the CFs, which forms the Zn_2GeO_4/CFs composites. For the comparison, lower (30% H_2O_2) or stronger (5 M HNO_3) oxidizing agent for pretreatment of CFs have been tested. As shown in Fig. 3D and E, due to the lower amount of surface defects on CFs surface, only small amount of Zn_2GeO_4 nanoparticles are covered onto CFs using 30% H_2O_2 as oxidizing agent. In contrast, using 5 M HNO_3 for pretreatment of CFs, large amount of Zn_2GeO_4 nanoparticles covered on the surface of CFs can be observed. These Zn_2GeO_4 nanoparticles are uniformly and compactly grown to form an open porous and rough structure.

The band gap of the as-prepared Zn_2GeO_4/CFs was determined to be ~4.6 eV on the basis of the UV-vis diffusion reflectance spectrum, as shown in the inset of Fig. 4A. The potential of edges of the valence band (E_{VB}) and conduction band (E_{CB}) for the Zn_2GeO_4 nanorods are estimated to be 3.8 and −0.7 V (*vs.* NHE) *via* the Mulliken electronegativity method, respectively.[19] The holes in the valence band (h_{vb}^+) would oxidize water and/or part of *p*-toluidine in the water system. The excited electrons in the conduction band (e_{cb}^-) are trapped by molecular oxygen (O_2) to form superoxide ions ($O_2^{\bullet -}$). The e_{cb}^- has enough potential to oxidated *p*-toluidine (half-peak potential $E_{1/2}^{red}$ = +0.16 V *vs.* SHE) (Fig. 4B).[20] The products during the photocatalytic oxidation were determined by Liquid Chromatography-Mass Spectrometry (LC-MS) analysis. As shown in Fig. 4C, the relative retention time (RRT) of chromatographic peak of normal *p*-toluidine is located at 2.6 min. After adding Zn_2GeO_4/CFs into reactive system, a new and intense chromatographic peaks located at 1.59 min can be observed after UV irradiation for 20 min. And the chromatographic peak (2.6 min) of *p*-toluidine is almost disappeared completely. It indicates *p*-toluidine has been transformed to *p*-nitrotoluene based on the Mass Spectrometry (MS) analysis (Fig. 4D). For analysis the synergistic effect on photocatalytic activity, the percent conversions (PC) for oxidation of *p*-toluidine over CFs, pure Zn_2GeO_4 and Zn_2GeO_4/CFs are tested under the same conditions. As shown in Fig. 4E, after UV irradiation for 20 min, the PC of *p*-toluidine is negligible over CFs which implies no photocatalytic ability for CFs. The PC is 83.28% for using Zn_2GeO_4 as catalyst. However, the PC can be further increased to 93.65% over Zn_2GeO_4/CFs. It indicates the presence of synergistic effect between Zn_2GeO_4 and CFs. The highest

PC for Zn_2GeO_4/CFs can be attributed: (i) the electron transfer between Zn_2GeO_4 and C will greatly retard the recombination of photo induced charge carriers and prolong electron lifetime.[21] As demonstrated by photocurrent photocurrent transient response and electrochemical impedance spectra (see Fig. S4 in ESI†). The higher photocurrent and smaller arc radius of Zn_2GeO_4/CFs demonstrates its higher charge separation efficiency; (ii) the CFs have an excellent adsorption capacity; (iii) the dispersion of Zn_2GeO_4 nanorods grown on CFs are improved, leading to the more reaction sites. In order to test the re-use performances of composite photocatalysts, the recycle experiment on the photocatalytic oxidation of *p*-toluidine solution is carried out. As shown in Fig. 4F, the efficiency of photocatalytic oxidation is still maintained without significant decline even after the six cycles. The excellent reuse performance of the Zn_2GeO_4/CFs may be resulted from the good binding property between Zn_2GeO_4 nanorods and carbon nanofibers.

Conclusions

In this work, the hexagonal Zn_2GeO_4 nanorods grown on the surface of CFs were prepared by a facile solvothermal method. The possible growth mechanism had been investigated by theoretical calculation and simulation experiment. The (113) crystal facet of Zn_2GeO_4 crystal attached to CFs surface was the most stable structure. This hypothesis also has been verified by growth of Zn_2GeO_4 on 2D flat surface of graphene. Due to the synergistic effect between photocatalytic activity of Zn_2GeO_4 and excellent adsorption capacity of CFs, the resultant Zn_2GeO_4/CFs composites exhibited excellent photocatalytic activity for oxidation of *p*-toluidine. We believe that this new assembly route in solution for nanostructured CFs at mild conditions will offer a new avenue to construct carbon-based catalytic materials for advanced applications in the fields of catalysis, energy, and environmental remediation.

Acknowledgements

This work was financially supported by the National Natural Science Foundation of China (51373155, 51133006), Public Technology Research Project of Zhejiang Province (2014C33G2060070) and "521 Talents Training Plan" in Zhejiang Sci-Tech University (ZSTU).

Notes and references

1 (*a*) G. Jiang, R. Wang, Y. Wang and X. Sun, *Powder Technol.*, 2011, **212**, 284–288; (*b*) R. Wang, G. Jiang, Y. Ding, Y. Wang, X. Sun, X. Wang and W. Chen, *ACS Appl. Mater. Interfaces*, 2011, **3**, 4154–4158; (*c*) G. Jiang, X. Zheng, Y. Wang, T. Li and X. Sun, *Powder Technol.*, 2011, **207**, 465–469; (*d*) R. Wang, G. Jiang, X. Wang, R. Hu, X. Xi, Y. Zhou, S. Bao, T. Tong, S. Wang, T. Wang and W. Chen, *Powder Technol.*, 2012, **228**, 258–263; (*e*) G. Jiang, R. Wang, X. Wang, R. Hu, X. Xi, Y. Zhou, S. Wang, T. Wang and W. Chen, *ACS Applied Mater. Interfaces*, 2012, **4**, 4440–4444.

2 (*a*) W. Chen, M. Chu, L. Gao, L. Mao, J. Yuan and W. Shangguan, *Appl. Surf. Sci.*, 2014, **324**, 432–437; (*b*) M.-C. Hsieh, G.-C. Wu, W.-G. Liu, W. A. Goddard III and C.-M. Yang, *Angew. Chem., Int. Ed.*, 2014, **53**, 14216–14220; (*c*) X. Zhang, B. Zhang, D. Huang, H. Yuan, M. Wang and Y. Shen, *Carbon*, 2014, **80**, 591–598.

3 (*a*) S. H. Hwang, J. Yun and J. Jang, *Adv. Funct. Mater.*, 2014, **24**, 7619–7626; (*b*) M. J. Llansola-Portoles, J. J. Bergkamp, D. Finkelstein-Shapiro, B. D. Sherman, G. Kodis, N. M. Dimitrijevic, D. Gust, T. A. Moore and A. L. Moore, *J. Phys. Chem. A*, 2014, **118**, 10631–10638; (*c*) J. Xu, T. J. K. Brenner, L. Chabanne, D. Neher, M. Antonietti and M. Shalom, *J. Am. Chem. Soc.*, 2014, **136**, 13486–13489.

4 S. Chen, H. Zhang, X. Yu and W. Liu, *Chin. J. Chem.*, 2011, **29**, 399–404.

5 M. Dinda, S. Chakraborty, S. Samanta, C. Bhatt, S. Maiti, S. Roy, Y. Kadam and P. K. Ghosh, *Environ. Sci. Technol.*, 2013, **47**, 10535–10540.

6 A. Hakki, R. Dillert and D. Bahnemann, *Catal. Today*, 2009, **144**, 154–159.

7 (*a*) J. L. Ferry and W. H. Glaze, *Langmuir*, 1998, **14**, 3551; (*b*) S. O. Flores, O. Rios-Bernij, M. A. Valenzuela, I. Córdova, R. Gómez and R. Gutiérrez, *Top. Catal.*, 2007, **44**, 507.

8 D. Sun, L. Ye and Z. Li, *Appl. Catal., B*, 2015, **164**, 428–432.

9 (*a*) M. Zhang, C. Chen, W. Ma and J. Zhao, *Angew. Chem., Int. Ed.*, 2008, **47**, 9730–9733; (*b*) V. Jeena and R. S. Robinson, *Chem. Commun.*, 2012, **48**, 299–301.

10 S. Song, M. Xia, Z. He, H. Ying, B. Lü and J. Chen, *J. Hazard. Mater.*, 2014, **144**, 532–537.

11 (*a*) Q. Liu, Z.-X. Low, L. Li, A. Razmjou, K. Wang, J. Yao and H. Wang, *J. Mater. Chem. A*, 2013, **1**, 11563–11569; (*b*) Q. Liu, Y. Zhou, J. Kou, X. Chen, Z. Tian, J. Gao, S. Yan and Z. Zou, *J. Am. Chem. Soc.*, 2010, **132**, 14385–14387; (*c*) G. Jiang, B. Tang, X. Li, Z. Wei, X. Wang, W. Chen, J. Wan and L. Shen, *Powder Technol.*, 2014, **251**, 37–40; (*d*) W. Zhao, C. Zhang, Y. Shi, R. Wu and B. Zhang, *Dalton Trans.*, 2015, **44**, 75–82; (*e*) Z.-Y. Xie, H.-L. Lu, Y. Zhang, Q.-Q. Sun, P. Zhou, S.-J. Ding and D. W. Zhang, *J. Alloys Compd.*, 2015, **619**, 368–371.

12 (*a*) J. Huang, K. Ding, Y. Hou, X. Wang and X. Fu, *ChemSusChem*, 2008, **1**, 1011–1019; (*b*) A. Abdukayum, J.-T. Chen, Q. Zhao and X.-P. Yan, *J. Am. Chem. Soc.*, 2013, **135**, 14125–14133; (*c*) J. Huang, K. Ding, Y. Hou, X. Wang and X. Fu, *ChemSusChem*, 2008, **1**, 1011–1019; (*d*) N. Zhang, S. Ouyang, P. Li, Y. Zhang, G. Xi, T. Kako and J. Ye, *Chem. Commun.*, 2011, **47**, 2041–2043; (*e*) M. Yang, Y. Ji, W. Liu, Y. Wang and X. Liu, *RSC Adv.*, 2014, **4**, 15048–15054.

13 (*a*) H. Tong, S. Ouyang, Y. Bi, N. Umezawa, M. Oshikiri and J. Ye, *Adv. Mater.*, 2012, **24**, 229–251; (*b*) G. Jiang, X. Wang, Z. Wei, X. Li, X. Xi, R. Hu, B. Tang, R. Wang, S. Wang, T. Wang and W. Chen, *J. Mater. Chem. A*, 2013, **1**, 2406–2410; (*c*) W. Guo, F. Zhang, C. Lin and Z. L. Wang, *Adv. Mater.*, 2012, **24**, 4761–4764; (*d*) G. Jiang, X. Li, Z. Wei, T. Jiang, X. Du and W. Chen, *Powder Technol.*, 2014, **261**, 170–175.

14 G. Jiang, X. Li, Z. Wei, T. Jiang, X. Du and W. Chen, *Powder Technol.*, 2014, **260**, 84–89.

15 M. Yang and X. Jin, *J. Cent. South Univ.*, 2014, **21**, 2837–2842.
16 Y. Luo, J. Jiang, W. Zhou, H. Yang, J. Luo, X. Qi, H. Zhang, D. Y. W. Yu, C. M. Li and T. Yu, *J. Mater. Chem.*, 2012, **22**, 8634–8640.
17 (*a*) J. Gou, B. Minaie, B. Wang, Z. Liang and C. Zhang, *Comput. Mater. Sci.*, 2004, **31**, 225–236; (*b*) A. Alipour Skandani, R. Zeineldin and M. Al-Haik, *Langmuir*, 2012, **28**, 7872–7879; (*c*) J. Goua, Z. Liang, C. Zhang and B. Wang, *Composites, Part B*, 2005, **36**, 524–533.
18 J. Song, S. A. Kulinich, J. Yan, Z. Li, J. He, C. Kan and H. Zeng, *Adv. Mater.*, 2013, **25**, 5750–5755.
19 (*a*) L. Ye, J. Liu, C. Gong, L. Tian, T. Peng and L. Zan, *ACS Catal.*, 2012, **2**, 1677–1683; (*b*) M. A. Butler and D. S. Ginley, *J. Electrochem. Soc.*, 1978, **125**, 228–232.
20 H. Tada, T. Ishida, A. Takao and S. Ito, *Langmuir*, 2004, **20**, 7898–7900.
21 (*a*) S. Sakthivel and H. Kisch, *Angew. Chem., Int. Ed.*, 2003, **42**, 4908–4911; (*b*) B. Jiang, C. Tian, Q. Pan, Z. Jiang, J. Wang, W. Yan and H. Fu, *J. Phys. Chem. C*, 2011, **115**, 23718–23725.